High speed miniature motorized endoscopic probe for optical frequency domain imaging

Li, J.A.; de Groot, M.; Helderman, F.; Mo, J.; Daniels, J.M.A.; Grünberg, K.; Sutedja, G.T.; de Boer, J.F.

published in
Optics Express
2012

DOI (link to publisher)
10.1364/OE.20.024132

document version
Publisher's PDF, also known as Version of record

High speed miniature motorized endoscopic probe for optical frequency domain imaging

Jianan Li,[1] Mattijs de Groot,[1] Frank Helderman,[1] Jianhua Mo,[1] Johannes M. A. Daniels,[2] Katrien Grünberg,[3] Tom G. Sutedja,[2] and Johannes F. de Boer[1,*]

[1]*Institute for Lasers, Life and Biophotonics Amsterdam, Department of Physics and Astronomy, VU University Amsterdam, De Boelelaan 1081, 1081 HV Amsterdam, The Netherlands*
[2]*VU University Medical Center, Department of Pulmonary Diseases, De Boelelaan 1117, Amsterdam, The Netherlands.*
[3]*VU University Medical Center, Department of Pathology, De Boelelaan 1117, Amsterdam, The Netherlands.*
**jfdeboer@few.vu.nl*

Abstract: We present a miniature motorized endoscopic probe for Optical Coherence Tomography with an outer diameter of 1.65 mm and a rotation speed of 3,000–12,500 rpm. This is the smallest motorized high speed OCT probe to our knowledge. The probe has a motorized distal end which provides a significant advantage over proximally driven probes since it does not require a drive shaft to transfer the rotational torque to the distal end of the probe and functions without a fiber rotary junction. The probe has a focal Full Width at Half Maximum of 9.6 µm and a working distance of 0.47 mm. We analyzed the non uniform rotation distortion and found a location fluctuation of only 1.87° in repeated measurements of the same object. The probe was integrated in a high-speed Optical Frequency Domain Imaging setup at 1310 nm to acquire images from ex vivo pig lung tissue through the working channel of a human bronchoscope.

OCIS codes: (170.2150) Endoscopic imaging; (170.4500) Optical coherence tomography.

References and links

1. D. Huang, E. A. Swanson, C. P. Lin, J. S. Schuman, W. G. Stinson, W. Chang, M. R. Hee, T. Flotte, K. Gregory, C. A. Puliafito, and J. G. Fujimoto, "Optical coherence tomography," Science **254**(5035), 1178–1181 (1991).
2. S. H. Yun, G. J. Tearney, B. J. Vakoc, M. Shishkov, W. Y. Oh, A. E. Desjardins, M. J. Suter, R. C. Chan, J. A. Evans, I. K. Jang, N. S. Nishioka, J. F. de Boer, and B. E. Bouma, "Comprehensive volumetric optical microscopy in vivo," Nat. Med. **12**(12), 1429–1433 (2007).
3. G. J. Tearney, M. E. Brezinski, B. E. Bouma, S. A. Boppart, C. Pitris, J. F. Southern, and J. G. Fujimoto, "In vivo endoscopic optical biopsy with optical coherence tomography," Science **276**(5321), 2037–2039 (1997).
4. Z. Yaqoob, J. Wu, E. J. McDowell, X. Heng, and C. Yang, "Methods and application areas of endoscopic optical coherence tomography," J. Biomed. Opt. **11**(6), 063001 (2006).
5. T. Q. Xie, H. K. Xie, G. K. Fedder, and Y. T. Pan, "Endoscopic optical coherence tomography with a modified microelectromechanical systems mirror for detection of bladder cancers," Appl. Opt. **42**(31), 6422–6426 (2003).
6. S. Han, M. V. Sarunic, J. Wu, M. Humayun, and C. H. Yang, "Handheld forward-imaging needle endoscope for ophthalmic optical coherence tomography inspection," J. Biomed. Opt. **13**(2), 020505 (2008).
7. G. J. Tearney, S. Waxman, M. Shishkov, B. J. Vakoc, M. J. Suter, M. I. Freilich, A. E. Desjardins, W. Y. Oh, L. A. Bartlett, M. Rosenberg, and B. E. Bouma, "Three-dimensional coronary artery microscopy by intracoronary optical frequency domain imaging," J. Am. Coll. Cardiovasc. Imaging **1**(6), 752–761 (2008).
8. A. M. Rollins, R. Ung-Arunyawee, A. Chak, R. C. Wong, K. Kobayashi, M. V. Sivak, Jr., and J. A. Izatt, "Real-time in vivo imaging of human gastrointestinal ultrastructure by use of endoscopic optical coherence tomography with a novel efficient interferometer design," Opt. Lett. **24**(19), 1358–1360 (1999).
9. P. R. Herz, Y. Chen, A. D. Aguirre, K. Schneider, P. Hsiung, J. G. Fujimoto, K. Madden, J. Schmitt, J. Goodnow, and C. Petersen, "Micromotor endoscope catheter for in vivo, ultrahigh-resolution optical coherence tomography," Opt. Lett. **29**(19), 2261–2263 (2004).
10. M. Tsuboi, A. Hayashi, N. Ikeda, H. Honda, Y. Kato, S. Ichinose, and H. Kato, "Optical coherence tomography in the diagnosis of bronchial lesions," Lung Cancer **49**(3), 387–394 (2005).
11. D. Lorenser, X. Yang, R. W. Kirk, B. C. Quirk, R. A. McLaughlin, and D. D. Sampson, "Ultrathin side-viewing needle probe for optical coherence tomography," Opt. Lett. **36**(19), 3894–3896 (2011).

#172814 - $15.00 USD Received 19 Jul 2012; revised 20 Sep 2012; accepted 1 Oct 2012; published 8 Oct 2012

12. W. Kang, H. Wang, Z. Wang, M. W. Jenkins, G. A. Isenberg, A. Chak, and A. M. Rollins, "Motion artifacts associated with in vivo endoscopic OCT images of the esophagus," Opt. Express **19**(21), 20722–20735 (2011).
13. P. H. Tran, D. S. Mukai, M. Brenner, and Z. Chen, "In vivo endoscopic optical coherence tomography by use of a rotational microelectromechanical system probe," Opt. Lett. **29**(11), 1236–1238 (2004).
14. S. Liang, A. Saidi, J. Jing, G. Liu, J. Li, J. Zhang, C. Sun, J. Narula, and Z. Chen, "Intravascular atherosclerotic imaging with combined fluorescence and optical coherence tomography probe based on a double-clad fiber combiner," J. Biomed. Opt. **17**(7), 070501 (2012).

1. Introduction

Optical Coherence Tomography (OCT) is a powerful optical technique for high resolution in vivo imaging of tissue morphology [1]. The Optical Frequency Domain Imaging (OFDI) implementation of OCT has shown great potential for comprehensive in vivo imaging of large volumes [2]. A critical research topic in OFDI is the development of high speed high resolution miniature probes for endoscopic in vivo imaging. Optical fiber and gradient-index (GRIN) lens designs are commonly used to deliver and focus light at the distal end of the catheter [3]. Referring to the direction of the imaging beam relative to the catheter itself, fiber based miniature OCT probes can be roughly classified into two categories: forward-viewing catheters, in which the imaging beam exits along the direction of the catheter; and side-viewing catheter, in which the imaging beam exits perpendicularly to the direction of the catheter [4]. While forward-viewing catheters play a role in fields such as bladder and ophthalmic imaging [5, 6], side-viewing catheters are utilized widely for imaging within hollow organs, from arteries to esophagus as well as colon and lung [7–10].

For rotational side-viewing OCT catheters, circumferential scanning can be implemented in two ways [4]: proximal scanning or distal scanning. For proximal scanning catheters, a motor placed outside the human body at the proximal end transfers rotational torque to the distal end by a drive shaft. A fiber optic rotary junction (FORJ) couples the light from the stationary to the rotating distal end. This approach enables thin probe designs down to 300 µm diameter [11]. However, a rotating flexible fiber in a stationary sheath commonly creates non-uniform rotation distortion (NURD) originating from friction in (sharp) bends [12]. Moreover, commercially available fiber optic rotary junctions for single mode fibers cannot rotate faster than 5000 rpm. Distal scanning probes use a miniature scanning module, for instance, a micromotor at the distal end of the probe to carry out circular scanning [13]. This design, though challenged by several engineering difficulties, has several advantages. A fiber rotary junction becomes obsolete. Drive shaft friction induced non-uniform rotation distortion can be avoided and higher scanning speeds can be achieved. Furthermore, such designs enable the possibility of combining OCT with other optical imaging techniques in a multimodality system, in which more complicated fiber designs such as double clad fibers may be used without the complication of a FORJ [14].

In this paper we present a miniature probe that integrates a micromotor in the distal end. Together with our OFDI system, we are able to acquire 3D data continuously at a speed of 208 frames per second. Results of ex vivo pig lung imaging experiment are demonstrated. The outer diameter of the probe is 1.65 mm.

2. Endoscopic probe

Figure 1(a) shows the design of our catheter. A single mode SM28 fiber is glued to a GRIN lens (GRINTECH, LFRL, 0.5 mm diameter) by index matching adhesive (Norland 89). It is encapsulated by a 1.35 mm outer diameter polymer sheath (Pebax®). At the end a piece of 1.65 mm diameter closed sheath is connected, with a 1 mm diameter micromotor (purchased from Kinetron and reassembled by ourselves) placed centrally inside. A spherical mirror is attached to the motor's axle in advance. The curvature (radius = 12.11 mm) of the mirror is selected to partially compensate astigmatism due to the presence of the sheath, which means instead of a single uniform waist there are still two separate narrowest positions for the two orthogonal directions (azimuthal and longitudinal) of the beam. This is simulated in Zemax,

#172814 - $15.00 USD Received 19 Jul 2012; revised 20 Sep 2012; accepted 1 Oct 2012; published 8 Oct 2012

illustrated in Fig. 2 and shown in Table 1. The tilt angle of the mirror is 40°, which is a balance between normal incidence condition and minimal back reflection from the sheath. The four electrical wires of the motor are bundled before the imaging window, eclipsing 1/10 of the view angle within the overall 2π circle. The total resistance of the catheter is 6 Ω, of which 5 Ω is from the wires. The low voltage driving signals are a sine and a cosine wave, which share a common ground, and have amplitude of 1.2 Vrms. The low voltage driving currents increase patient safety. Moreover, the driving currents are galvanically separated from the controller, the electrical wires of the motor are insulated and the volume resistivity of the sheath is 10^9 Ω·cm. The catheter is connected to the OCT system through a combined optical and electronic connector. When disconnected, sterilization of the whole catheter can be performed.

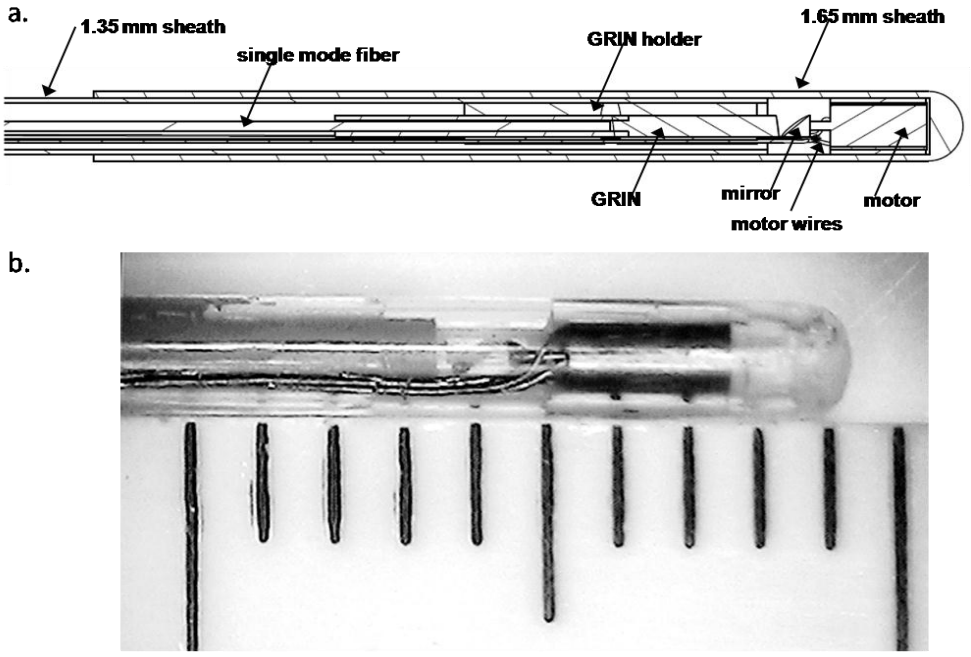

Fig. 1. (a) Drawing and (b) Photo of miniature catheter. Tick marks are separated by 1 mm.

We quantified the lateral resolution of the catheter by perpendicularly scanning a knife edge across the waist of the focusing beam and measuring the optical power after the knife edge. The profile of light intensity distribution at the beam waist was determined by taking the first order derivative of the optical power. The result is shown in Fig. 3. For the Y-Waist, a FWHM of 9.6 μm was measured, which indicates relatively high lateral resolution and short focal length.

#172814 - $15.00 USD Received 19 Jul 2012; revised 20 Sep 2012; accepted 1 Oct 2012; published 8 Oct 2012

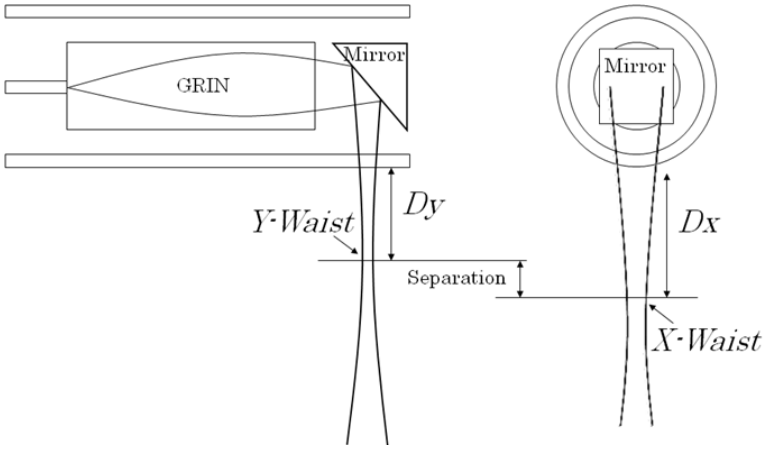

Fig. 2. Separation of X and Y waists.

Table 1. FWHM of the beam at different location. D is determined from the outer surface of the catheter sheath. The X-waist is situated at D = 0.54 mm; The Y-waist is situated at D = 0.40 mm. The X and Y Rayleigh lengths are 228 μm and 137 μm, respectively. All values are calculated assuming water (n = 1.333) around the catheter.

D (mm)	FWHM-X (μm)	FWHM-Y (μm)
0.10	20.3	17.2
0.20	17.3	13.2
0.30	14.7	10.2
0.40	12.6	8.9
0.47	11.7	9.5
0.54	11.4	11.2
0.60	11.6	13.1
0.70	12.9	17.0
0.80	15.0	21.4
0.90	17.7	25.9

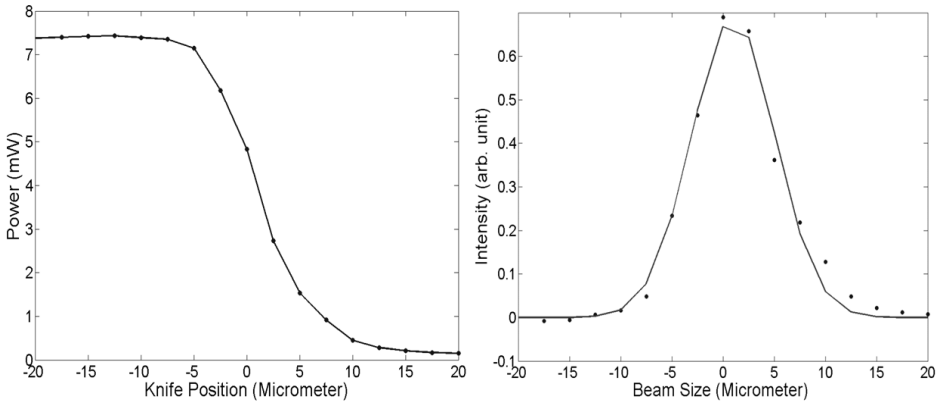

Fig. 3. Beam size characterization by knife edge test.

We carefully controlled the whole fabrication process to reduce optical power loss in the catheter as well as reflection that couples back into the system as ghost lines. We measured a total single pass power loss of 26% throughout the whole catheter. Excess reflection at each interface that couples back into the single mode fiber were measured and shown in Table 2.

#172814 - $15.00 USD Received 19 Jul 2012; revised 20 Sep 2012; accepted 1 Oct 2012; published 8 Oct 2012

Table 2. Excess reflection at each interface in the catheter. The catheter was placed in air. The measurement was carried out while the motor was rotating, thus the last three results show as ranges rather than constant values.

Surface	Fiber-GRIN	GRIN-Air	Mirror	Sheath-Inner	Sheath-Outer
Reflection (dB)	–51	–87	–87 - –77	–77 - –72	–72 - –62

Another issue which deserves close examination is the non-uniform rotation distortion. For quantitative characterization we manufactured a calibration object, a transparent hollow cylinder with 12 markers equally carved on its outer surface. The catheter was then inserted into this object to acquire images of those markers. At a speed of 52 fps, we recorded images for five seconds. The mean position of each marker in these 260 frames was analyzed and plotted in Fig. 4. The standard deviation around the mean was calculated. Averaged over the 10 marker positions, the standard deviation was 1.87°.

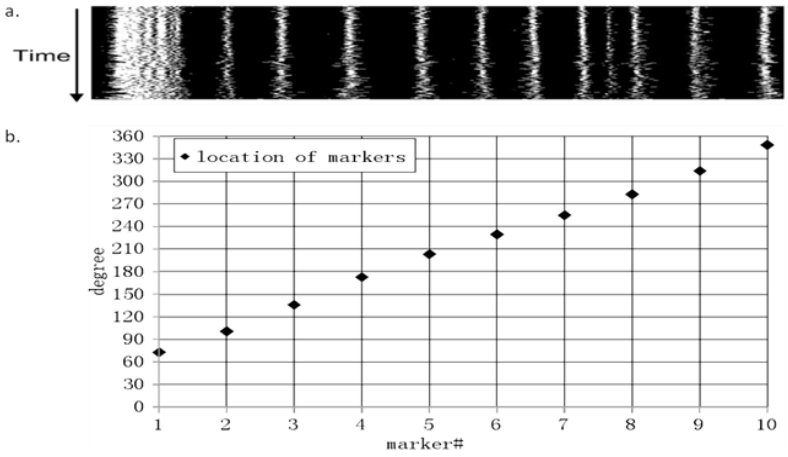

Fig. 4. Non-uniform rotation distortion measurement. (a) Evolution of location of markers within five seconds. Due to the presence of the motor wires, only 10 of the total 12 markers are clearly visible. Between marker 7 and 8 there is a weak spurious reflection, due to some dirt on the surface of the catheter sheath that casted a shadow. (b) The mean location of each marker throughout 260 frames in unit of degree.

3. Optical frequency domain imaging

The catheter was integrated in the sample arm of our OFDI system as shown schematically in Fig. 5. Light from a 1310 nm swept source (Axsun, 18 mW output, 50 kHz sweep rate) is delivered to both sample and reference arms by a 90/10 fiber coupler. Back reflected light enters a polarization diversity detection module and is detected by two dual balanced detectors (Thorlabs PDB130C). A high speed digitizer (Innovative Integration X5-400M) acquires data on the basis of a sweep trigger and k-clocking signals produced by the source. The catheter is controlled by a homemade controller which is synchronized with the laser sweep trigger via the counter output of a National Instruments PCIe6259 board.

The laser scanned over 102 nm, centered at 1310 nm, for which we measured an axial resolution of 15 μm in air after applying a Hann window. A sensitivity of 111 dB was measured on a mirror in a dummy sample arm with approximately 15 mW optical power while using a double pass attenuator of 48.6 dB. Along 5 mm full ranging depth we measured 3 dB signal roll-off.

#172814 - $15.00 USD Received 19 Jul 2012; revised 20 Sep 2012; accepted 1 Oct 2012; published 8 Oct 2012

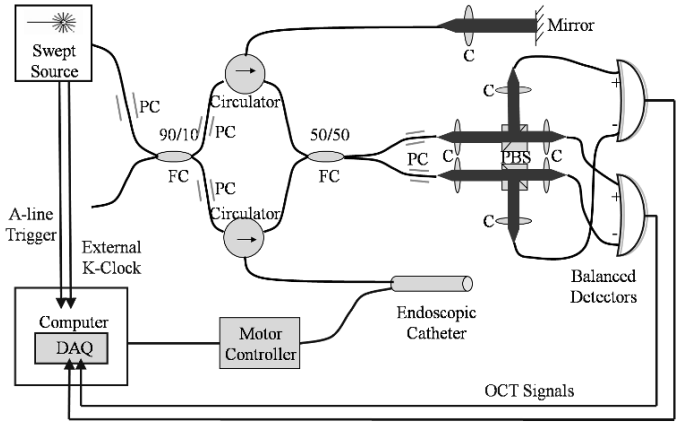

Fig. 5. Schematic of the OFDI system. PC: Polarization controller, C: Collimator, PBS: Polarizing beam splitter, FC: Fiber coupler.

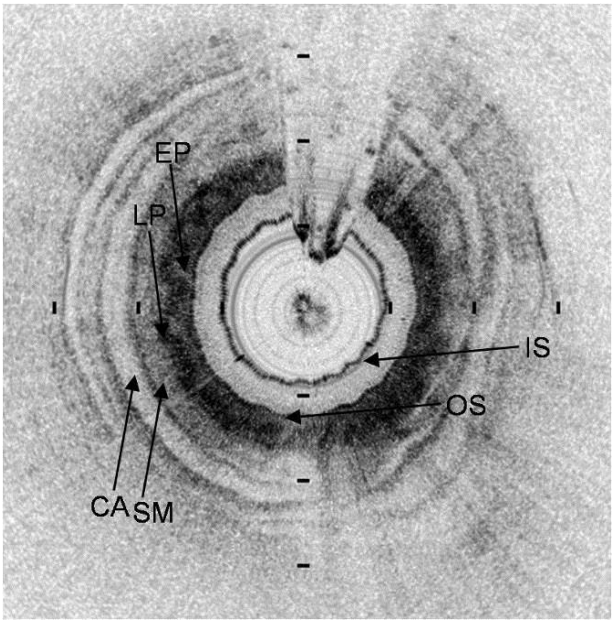

Fig. 6. OFDI image of pig bronchus at 52 fps (3120 rpm). Distance between adjacent markers is 0.5 mm. Position between 12 o'clock and 1 o'clock is blocked by the motor wires. EP: epithelium, LP: lamina propria, SM: submucosa, containing connective tissues and smooth muscle, CA: cartilage. IS/OS: inner/outer surface of catheter sheath. A video is available online (Media1).

To test the performance of the endoscopic catheter we conducted ex vivo pig bronchial imaging experiments. Fresh pig lung was obtained from the university laboratory animal centre. We inflated one of two lobes with compressed air and inserted the catheter through the endoscopic channel of a bronchoscope while maintaining the air pressure to prevent tissue collapse. The catheter was first placed at the region of interest and then pulled back for a certain length to acquire 3D volumetric data. The manual pull back speed was about 0.5 mm/s. We recorded several data sets with different duration. The catheter as well as the system was reliable and images were reproducible. Figure 6 is one frame of our OFDI image sequences. It contains 960 A-lines and shows several tissue layers of the pig bronchus in cross-section.

#172814 - $15.00 USD Received 19 Jul 2012; revised 20 Sep 2012; accepted 1 Oct 2012; published 8 Oct 2012

The rotation speed of the motor can be increased by at least a factor of four. We verified this by generating driving signals with the same amplitude but higher frequency. For the catheter used in this study, we observed that at a speed of 208 fps (12,500 rpm) the motor can still make smooth uniform rotation. Figure 7 is an image of human fingers acquired at this speed with 240 A-lines per image. The catheter is held between the thumb and index finger. The deformation of the image, that is visible as the oscillating shape of the catheter sheath surfaces, is caused by the precession of the motor's axle. For the motor used here the space between the axle and the bearing has more play than required. This can be improved in the future.

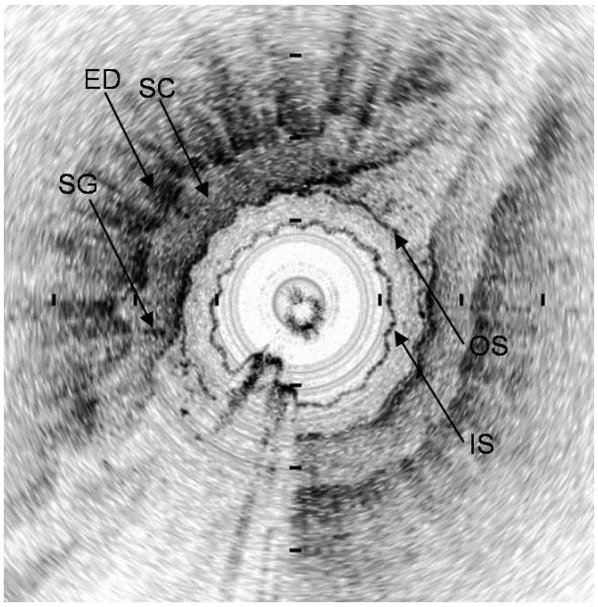

Fig. 7. Test of high speed rotation at 12,500 rpm – image obtained by holding the catheter between the thumb and index finger. The position between 6 o'clock and 7 o'clock is blocked by the motor wires. SC: stratum corneum, ED: epidermis, SG: sweat gland. IS/OS: inner/outer surface of catheter sheath. A video is available online (Media2).

4. Conclusions

In summary, we developed a fiber based motorized distal scanning miniature probe for endoscopic OFDI imaging. It has a diameter of 1.65 mm, which to our knowledge is the smallest of this type. Implemented in our 1310 nm OFDI system, it is able to acquire 3D volumetric data up to speeds as high as 208 frames per second. We demonstrated its performance with imaging ex vivo pig bronchial tissue and a human finger. Its small dimension provides the potential for imaging smaller bronchi which cannot be reached by traditional bronchoscopes. The high imaging speed enables fast pull-back, which permits comprehensive imaging of large volumes on short time scales.

Acknowledgments

This research was supported by grants from The Foundation for Fundamental Research on Matter (FOM: 09NIG03) and the research program Vernieuwingsimpuls which is (partly) financed by the Netherlands Organization for Scientific Research (NWO). J. Li acknowledges D. van Iperen, H. Voet, and J. Bouwman for their help on the development of a miniature catheter; J. Weda and B. Braaf for their advice and assistance.

#172814 - $15.00 USD Received 19 Jul 2012; revised 20 Sep 2012; accepted 1 Oct 2012; published 8 Oct 2012